

Angle Metrology of Dispersion Prisms

W. T. Estler (2) and Y. H. Queen

Precision Engineering Division

National Institute of Standards and Technology

Gaithersburg, MD 20899 USA

Tel: 301-975-3483, Fax 301-975-5360, e-mail: estler@nist.gov

Abstract

We present a new technique for calibrating the apex angles of dispersion prisms, which are used in the measurement of the index of refraction of optical glasses. The new method requires only a phase measuring interferometer, together with an electronic autocollimator, and eliminates the need for a rotary or indexing table. The apex angles of a nominally equilateral prism of fused silica were measured and the results compare favorably with a traditional calibration using an indexing table comparator.

Keywords: angular measurement, index of refraction, calibration

1. INTRODUCTION

Designers of complex lens systems for optical photolithography need to know the index of refraction of the lens materials (typically fused silica) with uncertainties approaching one part in 10^6 . The index of refraction of optical glasses is commonly measured by a technique known as minimum deviation, as illustrated in Figure 1. As a nearly equilateral prism (called a *dispersion prism*) of the material of interest is rotated about an axis normal to the plane of the figure, the angular deviation of a light ray incident as shown will pass through a minimum. This minimum deviation occurs when the path of the light ray through the prism is parallel to the base, as shown in Figure 1.

Denoting the angle of minimum deviation by φ_{\min} , and the index of refraction of the glass by n_g , a straightforward analysis [1,2] then shows that

$$n_g = \frac{\sin[(\varphi_{\min} + A)/2]}{\sin(A/2)}, \quad (1)$$

where A is the prism apex angle. The deviation φ_{\min} is typically measured with a prism spectrometer fitted with a

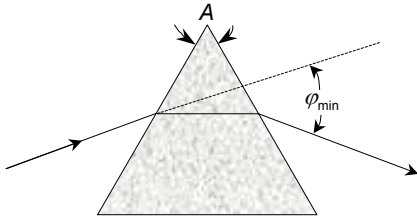


Figure 1. The path of minimum deviation for a ray of light through a dispersion prism. The prism apex angle is A , and the angular deviation is φ_{\min} .

high-accuracy angle encoder, while the apex angle A must be separately calibrated. Clearly, the uncertainty of such an index measurement is limited by uncertainties in the measurements of the angles φ_{\min} and A . For fixed φ_{\min} the sensitivity to apex angle error is

$$\frac{dn_g}{dA} = \frac{1}{2} \sin(\varphi_{\min}/2) \csc^2(A/2). \quad (2)$$

For typical values of $n_g \approx 1.5$, $A \approx 60^\circ$, and $\varphi_{\min} \approx 37^\circ$ we then have $|dn_g/dA| \approx 0.65$ or $|dn_g/n_g| \approx 0.43 dA$. Thus, neglecting any uncertainty in the measurement of φ_{\min} , in order to measure the index of refraction to within one part in 10^6 requires:

$$|dA| \leq 2.3 \times 10^{-6} \text{ radians} \approx 0.5 \text{ arc-seconds}. \quad (3)$$

Angle measurements to this level of accuracy are near state-of-the-art for artifacts such as prisms and optical polygons [3].

2. OBSERVATIONS WHEN MEASURING FACE FLATNESS ERRORS OF A DISPERSION PRISM

At the National Institute of Standards and Technology (NIST) the most accurate calibrations of angle artifacts are carried out on the Advanced Automated Master Angle Calibration System (AAMACS), a fully automated system of highly repeatable, high-resolution indexing tables [3]. When measuring angles between nominally planar surfaces using high-resolution autocollimators, we have demonstrated fundamental limits to achievable uncertainty due to flatness errors of the reflecting surfaces [4].

As a rule of thumb, systematic, low spatial frequency figure errors of the order of $\lambda/20$ ($\lambda = 633 \text{ nm}$) can be expected to cause variations in the direction of the average surface normals, as measured by different autocollima-

tors, of a few tenths of an arc-second or approximately one microradian. For this reason, during the calibration of very high quality angular artifacts we routinely measure the face flatness errors using a well-characterized commercial phase measuring interferometer (PMI) system.

During the process of measuring the face flatness errors of a fused silica dispersion prism that was sent to NIST for calibration, we noticed that by performing small angular adjustments of the prism near the primary null that we could observe any one of three separate and distinct interferograms of similar contrast. One of these interferograms, of the size of the rectangular prism face, represented the flatness error of interest while the other two were of one-half aperture size coincident with the left and right halves, respectively, of the prism face. Figure 2 shows a photograph of the three fringe patterns.

3. DISPERSION PRISM GEOMETRY AND THE HALF-APERTURE INTERFEROGRAMS

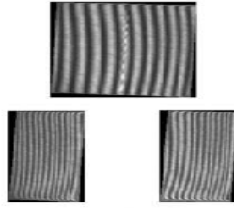


Figure 2. The three fringe patterns observed with a 60° dispersion prism and a Fizeau interferometer.

The origin of the two half-aperture interferograms can be understood by reference to Figure 3, which shows the relevant ray paths. The secondary fringe patterns (paths 1 and 2 in the figure) are caused by rays which enter the prism and return after three internal reflections, the first and last of which are total (and thus lossless). The angular separation of the interferograms results from a lack of

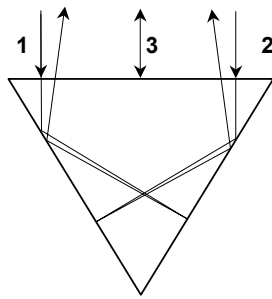


Figure 3. The three possible interferogram ray paths for a dispersion prism.

geometric perfection in the nominally equilateral prism. For a perfect prism, the three incident rays would each be retroreflected and the signals would overlap, in all likelihood confusing the PMI analysis software. For the prism we tested the angular separations of the images were on order of one or two arc-minutes

Now let the prism in Figure 3 be rotated through a small angle δ_1 so that ray path 1 is retroreflected. In this posi-

tion a half-aperture null interferogram will be observed on the PMI system and the resultant geometry may be understood by reference to Figure 4.

Assuming the prism to be nearly equilateral, we denote

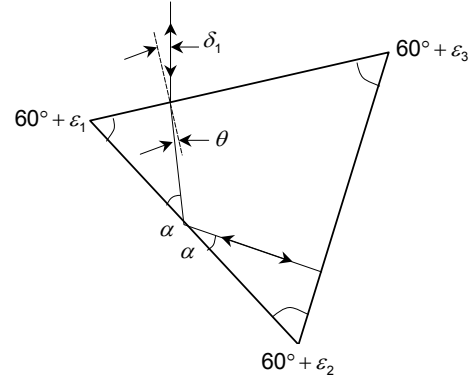


Figure 4. Prism orientation yielding one of the half-aperture interferograms. The angle δ_1 is exaggerated.

the apex angles by $60^\circ + \varepsilon_k$, $k = 1, 2, 3$. From the diagram we see that there are two triangles containing the unknown angle α . Summing the angles in these two triangles yields the relations:

$$\begin{aligned} 180^\circ &= \alpha + (60^\circ + \varepsilon_1) + (90^\circ - \theta) \\ 180^\circ &= \alpha + (60^\circ + \varepsilon_2) + 90^\circ. \end{aligned} \quad (4)$$

Subtracting and rearranging yields:

$$\theta = \varepsilon_1 - \varepsilon_2. \quad (5)$$

The refraction angle θ is related to the angle of incidence δ_1 by Snell's Law: $\sin \delta_1 / \sin \theta = n_g / n_{\text{air}}$. Setting $n_{\text{air}} = 1$ and $\sin \delta_1 / \sin \theta \approx \delta_1 / \theta$ for small angles, (5) becomes:

$$\delta_1 = n_g (\varepsilon_1 - \varepsilon_2). \quad (6)$$

If the prism is now re-oriented so that ray path 2 is retroreflected, a similar analysis yields the relation

$$\delta_2 = n_g (\varepsilon_2 - \varepsilon_3), \quad (7)$$

where the angle δ_2 is defined by analogy with δ_1 , with a change of algebraic sign.

Equations (6) and (7) provide two relationships among the three unknown angles $(\varepsilon_1, \varepsilon_2, \varepsilon_3)$. A third relationship follows from the *angle closure constraint* [5,6]:

$$\varepsilon_1 + \varepsilon_2 + \varepsilon_3 = 0. \quad (8)$$

The three equations (6-8) can then be solved to yield:

$$\varepsilon_1 = \frac{2\delta_1 + \delta_2}{3n_g} \quad (9a)$$

$$\varepsilon_2 = \frac{-\delta_1 + \delta_2}{3n_g} \quad (9b)$$

$$\varepsilon_3 = \frac{-\delta_1 - 2\delta_2}{3n_g}. \quad (9c)$$

Measurement of the two angles δ_1 and δ_2 thus suffices to completely determine the apex angles of the prism, provided that the refractive index n_g is known *a priori*. Note that both angles δ_1 and δ_2 are measured using one face of the prism. Additional (partially redundant) data can be obtained by repeating the measurements using the other two prism faces.

The form of the data equations (6) and (7) shows that the angles δ_1 and δ_2 each encode an *optical angle difference* (OAD) $n_g \Delta \varepsilon$. Such a quantity is analogous to the familiar *optical path difference* (OPD) $n_g \Delta x$ measured for a physical path difference Δx in conventional interferometry. The technique is an internal comparator method in which the prism apex *optical angles* $n_g \varepsilon_k$ are intercompared within the glass. The dependence upon the refractive index suggests two types of practical application:

- If the refractive index n_g is known with an acceptable uncertainty, then the prism apex angles can be calibrated according to Eqs. (9).
- If n_g is unknown, the results from Eqs.(9) can be combined with a separate external apex angle calibration and the results used to calculate n_g . A simple technique for such an external calibration, using only an accurate autocollimator, has been described by Rao [7].

4. EXPERIMENTAL TEST OF CONCEPT

The angles δ_1 and δ_2 can be conveniently measured using the setup shown schematically in Figure 5. The prism is mounted on a small rotation stage together with an auxiliary plane mirror. A high-resolution (0.05 arc-second) electronic autocollimator aligned to the plane mirror measures the amount of stage rotation as each of the three accessible interferograms is brought into null alignment with the PMI reference transmission flat. The precise angular positions of the three interferometric nulls are found by making several maps of the optical path difference (OPD) on either side of null. Computed tilt from

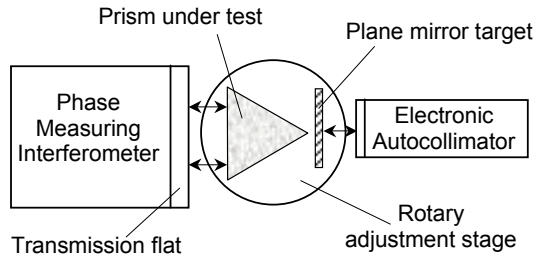


Figure 5. Experimental setup for prism apex angle measurement. The autocollimator measures the angular separation between the three interferometric nulls.

each of these maps (waves/aperture units) is then least-squares fit to the set of angular positions measured by the autocollimator. The null positions are then computed

from the zero crossings of the fit lines. The differences between the null position of the full-aperture interferogram and each of the two sub-aperture interferograms yield the angles δ_1 and δ_2 of interest.

Table 1 shows the results of six measurements of the apex angles of a UV-grade fused silica dispersion prism with 50 mm \times 25 mm faces. The angles were computed from measured values of δ_1 and δ_2 using Eqs.(9) and the value $n_g \approx 1.457$ at $\lambda = 633$ nm, the PMI wavelength [8].

The apex angles were measured using each of the three prism faces as the entrance face, and the entire measurement sequence repeated twice.

The apex labeled "A" is the angle of interest to the customer for the use of the prism in a high-accuracy minimum deviation determination of the refractive index. This apex angle was independently calibrated using the AAMACS system. Apex A was measured in both "top up" and "top down" positions. In each position the apex angle was sequentially compared with a contiguous set of 50 nominally-equal comparator angles in a procedure called *partial closure*. The AAMACS calibration yielded:

$$(A - 60^\circ)_{\text{AAMACS}} = (80.0 \pm 0.4) \text{ arc-seconds}, \quad (10)$$

where the $k=2$ expanded uncertainty of 0.4" is dominated by uncertainty due to flatness errors of the prism faces.

Run	Entrance face	Angle Deviations from 60° (arc-sec)		
		Apex A	Apex B	Apex C
1	AB	80.4	-49.6	-30.8
	AC	81.1	-49.9	-31.2
	BC	81.1	-49.9	-31.2
2	AB	79.5	-48.9	-30.6
	AC	81.7	-50.5	-31.2
	BC	80.5	-51.7	-28.8
Average		80.7	-50.1	-30.6
Std. Deviation		0.8	0.9	0.9

Table 1. Results of dispersion prism apex angle measurements using the setup of Figure 5. Prism material: UV-grade fused silica, $n_g \approx 1.457$ @ $\lambda = 633$ nm.

As seen from Table 1, the initial results are reasonably encouraging. The result for apex angle A is:

$$(A - 60^\circ)_{\text{TEST}} = (80.7 \pm 1.6) \text{ arc-seconds}, \quad (11)$$

where 1.6" is not the actual angle measurement uncertainty but rather a 2σ measure of reproducibility computed from the six measurement results. We stress this point because a complete uncertainty budget must address systematic effects and the effect of imperfect realization of the measurand. We turn to a brief discussion of these matters.

5. MEASUREMENT UNCERTAINTY

In these preliminary experiments we made no particular attempt to optimize the measurement procedure or to

minimize errors due to effects such as thermal drift or air turbulence. It is interesting to ask how well a prism might be calibrated under well-controlled conditions. Assuming an adequate thermal environment and measurement reproducibility, the principal contributors to measurement uncertainty are (1) autocollimator errors, including realization of the unit and measurement noise; (2) imperfect realization of the measurand; (3) PMI error in the angular positions of the interferometric nulls; and (4) refractive index uncertainty.

Equations (9) show the explicit dependence of the prism apex errors on the measurement data from which the uncertainties can be evaluated using the formula for the propagation of error [9]. From (9a) for example, it is straightforward to show that the uncertainty in ε_1 due to autocollimator and refractive index uncertainties is:

$$u(\varepsilon_1) = \frac{1}{3n_g} \left[4u^2(\delta_1) + u^2(\delta_2) + \frac{(2\delta_1 + \delta_2)^2}{n_g^2} u^2(n_g) \right]^{1/2} \quad (12)$$

For UV-grade fused quartz at 633 nm, $u^2(n_g) \approx 10^{-8}$ and the last term can be neglected for angles within the range of the autocollimator. Assuming equal uncertainties for the two autocollimator measurements:

$$u^2(\delta_1) = u^2(\delta_2) = u_0^2,$$

Eq. (12) reduces to:

$$\begin{aligned} u(\varepsilon_1) &\approx \frac{\sqrt{5}}{3n_g} u_0 \\ &\approx 0.5u_0. \end{aligned} \quad (13)$$

The same result holds for $u(\varepsilon_3)$, while $u(\varepsilon_2) \approx 0.3u_0$, a slightly smaller value because both measured angles depend directly on ε_2 . From the specifications of the autocollimator used in the tests, $u_0 \approx 0.3''$ over the measurement range of $\pm 1000''$ so that $u(\varepsilon_1) = u(\varepsilon_3) \approx 0.2''$ and $u(\varepsilon_2) \approx 0.1''$. By taking a weighted mean of measurements through all three prism faces these results can be slightly improved.

A possible source of error arises from the use of Zernike polynomials whose X-axis tilt coefficients are plotted against the autocollimator data in order to detect, via zero crossings, the angular positions of the three interferometric nulls. The Zernike polynomials form an orthogonal set over a circular aperture, while in these experiments we fit to rectangular apertures. In the case of the half-width, through-the-glass interferograms, these rectangular apertures were off-axis as well. A series of numerical experiments using synthetic data showed that while the Zernike coefficients are sensitive to various rectangular maskings of the data, the effect on the zero crossing null positions, for surfaces dominated by power as were the faces of our test prism, is less than $0.1''$ and thus negligible.

A fundamental limitation on achievable uncertainty follows from the failure of real prisms to realize the measurand, defined to be the angle between surface normals of perfectly flat faces. PMI face maps for the prism used in these experiments showed each face to be concave and dominated by power ($z \propto x^2$) as illustrated in Figure 6.

Departures Δ from perfect planarity were in the range 20 nm to 60 nm. For such a prism, the closure constraint is violated and the face curvature will introduce a systematic error into the measurement results. In principle, be-

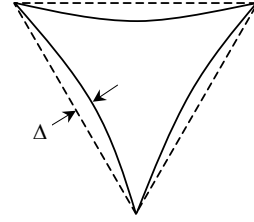


Figure 6. A prism with convex faces (exaggerated). The apex angles do not sum to 180° .

cause the shapes of the prism faces are measured by the PMI in the course of the experiment, one could use ray tracing to calculate the mean deviation of a ray bundle through the prism in the through-the-glass null positions, and thus to correct the autocollimator data for the mean face curvature. The limiting uncertainty, however, will be set by the unknown quality of the autocollimator's own beam forming optics.

6. ACKNOWLEDGEMENTS

We thank Dr. C. J. Evans for substantial contributions to this work.

7. REFERENCES

- [1] Nussbaum, A. and Phillips, R.A., 1976, "Contemporary Optics for Scientists and Engineers," Prentice-Hall, NY.
- [2] Hecht, E. and Zajac, A., 1973, "Optics" Addison-Wesley, Reading, MA.
- [3] Estler, W. T., and Queen, Y. H., 1993, "An Advanced Angle Metrology System", CIRP Annals, Vol. 41/1, p. 573.
- [4] Estler, W. T., Queen, Y. H., Gilsinn, D., and Pieczulewski, D., 1991, "Advanced Angle Metrology at the National Institute of Standards and Technology," Proc. of the ASPE 1991 Annual Conference.
- [5] Evans, C. J., Hocken, R. J., and Estler, W. T., 1996, "Self-Calibration: reversal, redundancy, error separation, and 'absolute testing'," CIRP Annals Vol. 45/2, p. 791.
- [6] Estler, W. T., 1998, "Uncertainty Analysis for Angle Calibrations Using Circle Closure," J. Res. Natl. Inst. Stand. Technol. **103**, 141-151.
- [7] Rao, S. M., 1997, "Method for measurement of the angles of an equilateral (60-deg) prism," Opt. Eng. **36**(5) 1508-1509.
- [8] Tables of n_g versus λ for fused silica can be found at: www.layertech.de/sio2-uv.htm (Layertec GmbH., Melling, Germany) and www.crystran.co.uk/sio2-ri.htm (CRYSTRAN Ltd., Dorset, UK).
- [9] ISO, 1993, *Guide to the Expression of Uncertainty in Measurement*, International Organization for Standardization, Geneva, Switzerland.